


Magnetic nanoparticle hyperthermia enhanced by a rotating field

Gabriele Barrera¹,* Paolo Allia¹, and Paola Tiberto

Advanced Materials Metrology and Life Sciences, Istituto Nazionale di Ricerca Metrologica (INRiM), 10135 Torino, Italy

 (Received 31 January 2024; revised 27 March 2024; accepted 17 May 2024; published 14 June 2024)

The heating efficiency of magnetite nanoparticles for therapeutic hyperthermia is shown to be substantially enhanced by applying a uniformly rotating magnetic field in place of a field directed along an axis, when all other factors are held constant. Optimization of the heating efficiency is actively pursued in order to keep the volume fraction of nanoparticles as low as possible, reducing the adverse effects emerging from nanoparticle accumulation in organs. The effect of a rotating magnetic field is calculated by solving rate equations for the magnetic moments of magnetite nanoparticles with predominant Néel relaxation and pictured as double-well systems. The model results in a simple expression for the power density generated by nanoparticles with random easy-axis directions. A thermal model of a tissue simulant is used to show that applying a rotating instead of a linear field permits us to more than halve the dose of nanoparticles needed to attain the target temperature in the tissue.

DOI: [10.1103/PhysRevApplied.21.064037](https://doi.org/10.1103/PhysRevApplied.21.064037)

I. INTRODUCTION

Magnetic nanoparticle hyperthermia has revealed to be a most promising challenging technique of precision medicine aimed at the cure of tumors [1–6]. The unique blend of physicochemical properties and of the physiological demands of tumor therapy has made this field of research complex to dominate as well as intriguing to investigate [7]; in fact, in recent years, a great effort has been conducted toward a comprehensive multifaceted vision of the problem.

Magnetic particle hyperthermia has originally attracted immediate attention because it does not involve the use of ionizing radiation or dangerous substances; moreover, it is based on rather simple physical principles, at least in principle [8–10]. Advances in fundamental knowledge have helped to clarify many initially obscure points, resulting in concurrent advances in therapy. Nowadays, it is known that oversimplified models of the magnetic response of nanoparticles (which is at the very basis of their efficacy as pointlike heat sources) should be definitely discarded in favor of a more refined description of the high-frequency magnetic behavior [9,11–13], and that *in vivo* treatments require an in-deep knowledge of the thermal effects produced by nanoparticles in the tissue in which they are placed [14,15].

Although important issues about the fundamental magnetic properties of nanoparticles and their physical interaction with living tissue can be considered as basically solved, a number of equally urgent requirements about the

optimization of their heating performance as well as their interaction with a patient's body and metabolism are still under discussion. Optimization of the specific loss power (SLP) of magnetic nanoparticles has recently been pursued at the level of general architecture of the therapy (e.g., by defining appropriate treatment plans [16]) as well as at the level of fundamental properties such as nanoparticle shape, size, and assembly [4,17,18]. Open issues preventing the diffusion of magnetic hyperthermia as a therapeutic tool include the difficulty of depositing an adequate dose (i.e., volume concentration) of particles at the tumor by targeted vehiculation in a fluid environment, as well as the weak heating performance of magnetic fluids available on the market, which contain a wide distribution of nanoparticle sizes [19]. The main aim of any recent activity in this field is, of course, to get the maximum heating efficiency using the lowest possible amount of nanoparticles in order to reduce potentially harmful side effects [19–21]. The need to keep the volume concentration as low as possible is clearly related to the adverse effects emerging from nanoparticle accumulation in organs and the problems posed by clearance [22,23], both of which are also remarkably dependent on nanoparticle size [24].

In principle, the SLP could be optimized either acting on the properties of the particles or acting on the ac driving field. The second strategy has the obvious advantage of making use of the nanoparticle materials already approved for medical use by the U.S. Food and Drug Administration (FDA) and the European Medicines Agency (EMA) [25]. However, a high heating efficiency of nanoparticles cannot be obtained by simply increasing the frequency and amplitude of the driving field, because of the emergence of

*Corresponding author: g.barrera@inrim.it

well-known detrimental effects when large magnetic fields of sufficiently high frequency are applied to healthy tissue [26,27]. Such physiological constraints greatly reduce the degrees of freedom available to the user; however, the performance of magnetic nanoparticles can still be optimized, and a significant reduction in their volume concentration can still be achieved, by acting on specific features of the magnetic field used to drive the nanoparticle magnetization at high frequency. The particle SLP has been shown to be improved by using combinations of ac and dc magnetic fields [28]. From a different standpoint, the beneficial effects of using trapezoidal or square ac field wave forms instead of the sinusoidal ones have been theoretically clarified [29,30] and experimentally verified [31].

In fact, in virtually all the existing or envisaged applications of magnetic nanoparticle hyperthermia, the driving field is directed along an axis (this is, of course, a rather easy configuration to deal with, because it is naturally generated by a single linear magnetizing coil). However, a magnetic field applied along an axis is not the best solution in the presence of magnetic nanoparticles evenly distributed in space, as is the case of nanoparticles placed at the desired target inside a living body.

In this work, it is proven that the heating efficiency is markedly enhanced by exciting the nanoparticles by means of a uniformly rotating magnetic field instead of a harmonic field directed along an axis. Use is made of the Néel magnetic relaxation scheme, which is appropriate to treat nanoparticles already immobilized in the malignant tissue [32,33]. In this framework, the magnetic response is dominated by energy-barrier crossing of magnetic moments on nanoparticles [9].

In recent years, magnetic particle hyperthermia resulting from the application of a uniformly rotating field of high frequency has been theoretically [34–36] and experimentally [37–40] studied; however, these works are focused on the power dissipated by a magnetic fluid, where the nanoparticle magnetization is either dominated by Brownian relaxation [36] or involves the concurrent effects of the Brown and Néel mechanisms [37,38,40], depending on particle size. The Brownian relaxation is expected to be negligible not only when the nanoparticles are immobilized but also in magnetic fluids at the experimentally explored frequencies (≥ 100 kHz) [39,41]. However, in the theoretical approaches involving Néel relaxation in fluids, a detailed treatment of the kinetics of magnetic moment redistribution is lacking. Moreover, the magnetic response of nanoparticles submitted to the uniformly rotating field is typically treated in the linear approximation (i.e., by focusing on the behavior of the dynamic magnetic susceptibility), which can be inadequate to picture the behavior of nanoparticles driven by the magnetic field amplitudes exploited in therapeutic practice [9].

Studying the heating efficiency of randomly dispersed magnetic nanoparticles the magnetic response of which is

dominated by Néel relaxation in living tissue needs a complex formalism and the concurrent use of magnetic and thermal models. To this aim, a thermal model referring to a specific living-body simulant and a detailed magnetic model based on the rate-equation treatment of energy-barrier crossing of magnetic moments are introduced and discussed in the following sections.

II. THERMAL MODEL OF A LIVING-TISSUE SIMULANT

The power density released by magnetic nanoparticles plays a central role in equations used to picture the bio-heat transfer in a living body. Such equations model—up to different levels of refinement—the inherently complicated process of local heating of a malignant tissue by magnetic nanoparticle hyperthermia. They include the pioneering Pennes equation [42] and other increasingly complex approaches such as the Chen-Holmes and the Weinbaum-Jiji-Lemons equations [43]. In all such treatments, the magnetic power density keeps the very same functional form and is considered to be the only important local source of heat (smaller effects related to metabolism often being neglected [43]).

In this work, the aim of which is to clarify the effects of an unconventional excitation of magnetic nanoparticles rather than to picture bioheat transfer in a specific malignant tissue, a simplified heating model of human tissue is adopted, consisting of an artificial simulant (a *phantom*), shaped in the form of a sphere of radius $b = 1$ cm and containing a volume fraction f_V of evenly distributed magnetite nanoparticles. The phantom is entirely surrounded by a nanoparticle-free medium; the convective boundary conditions at the interface ($r = b$) are related to the tissue-blood perfusion rate. It is assumed that pure Néel magnetic relaxation is the dominant source of heat generation, in line with the notion that magnetic nanoparticles are physically constrained by the host tissue, so that particle translation and/or rotation are suppressed [8,44].

In this case, and with the considered radial symmetry of the phantom, it is easy to show that the Pennes equation basically reduces to the standard radial Fourier equation with uniform thermal conductivity k and thermal diffusivity α_T :

$$\frac{\partial^2 T}{\partial r^2} + \frac{2}{r} \frac{\partial T}{\partial r} + \frac{P_{\text{in}}}{k} = \frac{1}{\alpha_T} \frac{\partial T}{\partial t}, \quad (1)$$

where T is the temperature increment above the starting temperature (assumed to be $T_0 = 310$ K) and the k and α_T parameters take values appropriate to typical tissue simulants: $k = 0.5 \text{ W m}^{-1} \text{ K}^{-1}$ and $\alpha_T = 1.4 \times 10^{-7} \text{ m}^2 \text{ s}^{-1}$ [9]. The input power density P_{in} is proportional to the volume concentration f_V of nanoparticles in the phantom ($0 \leq f_V \leq 1$). As pointed out elsewhere [9], the power

density is affected by the magnetic parameters of the nanoparticles, such as the saturation magnetization and the effective anisotropy constant. Both quantities are temperature dependent, so that in principle the term P_{in} in Eq. (1) implicitly depends on temperature, making the Fourier equation impossible to solve analytically. However, for limited temperature intervals (not exceeding 10–15°), as is typically the case for *in vivo* hyperthermia, the input power density can be considered constant to a good approximation.

The quantity P_{in} turns out to be remarkably affected by the type of high-frequency excitation of magnetic nanoparticles (e.g., by the shape of the driving-field wave form [29, 30]). In Sec. III, the effect of a uniformly rotating instead of linear magnetic field is discussed in the framework of Néel nanoparticle relaxation.

III. MODELING THE RESPONSE OF MAGNETIC NANOPARTICLES

We consider monodisperse single-core nanoparticles of pure stoichiometric magnetite (Fe_3O_4) with diameters D in the range of 9–16 nm and basically noninteracting. Such an assumption is justified by the low concentration of magnetic particles usually exploited in clinical applications of magnetic hyperthermia (of the order of 1% by volume or less [45]) and by the widespread presence of functionalized surfaces, both of which make the mean interparticle distance sufficiently large to significantly reduce dipolar coupling. The nanoparticles are typified by a dominant uniaxial anisotropy characterized by an effective constant K_{eff} that can include the effect of weak dipolar interactions as well [46], with random distribution of the easy axes in three dimensions.

In the main body of the work, the particle magnetization and magnetic anisotropy are assumed to take values independent of the particle size ($M_s = 350 \text{ emu/cm}^3$ and $K_{\text{eff}} = 3 \times 10^5 \text{ erg/cm}^3$, deemed to be representative of actual single-core magnetite particles around room temperature [47]). This simplifying assumption is justified by experimental evidence indicating that the effect of the particle size on the intrinsic magnetic properties is reduced in the considered range of D values [48,49]. Moreover, a small or even insignificant effect of size on both M_s and K_{eff} has been observed in Fe_3O_4 nanoparticles characterized by a particularly high crystal quality and stoichiometry as well as by a well-defined shape [49–52].

On the other hand, a significant role of nanoparticle surface on both M_s and K_{eff} has been found in a number of measurements [48,53–55], although particularly important effects have mainly been observed in very small particles [53,56]. It has been suggested [49] that size-dependent magnetic properties are more frequently observed in structurally or compositionally defective nanoparticles, as confirmed by simulations indicating that *intrinsic* surface

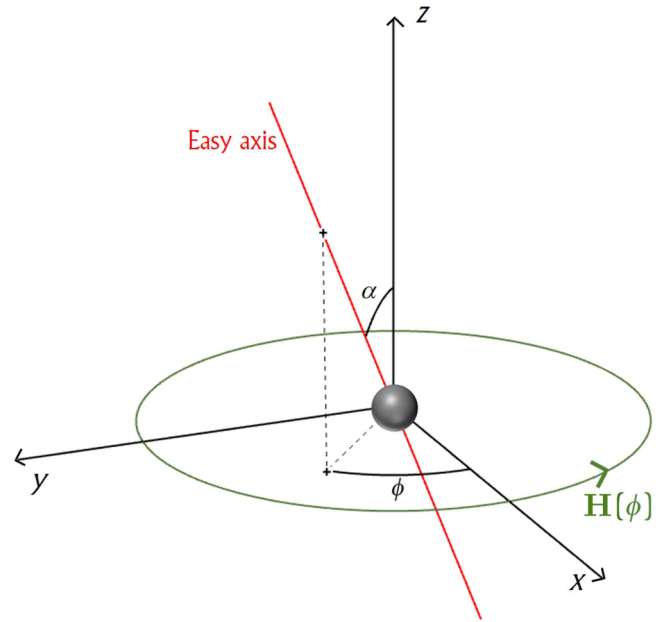


FIG. 1. The relation between the spherical coordinate angles α and ϕ and the rectangular x , y , and z axes. The magnetic field rotates uniformly counterclockwise in the x - y plane.

effects in ideal Fe_3O_4 particles are relevant only for sizes below about 5 nm. Nevertheless, in order to expand our predictions to cases in which size effects appear to play a non-negligible role on the magnetic properties, the present analysis is extended in the Appendix to magnetite nanoparticles characterized by an explicit size dependence of both M_s and K_{eff} based on experimental evidence [48,49].

The direction of the easy axis is defined by the angles α and ϕ , as shown in Fig. 1. The magnetic field lies in the x - y plane, where it uniformly rotates counterclockwise, and is generated by two orthogonal harmonic fields, applied, respectively, along the x and to the y axis, having the same frequency $f = 100 \text{ kHz}$ and time-dependent amplitudes $H_1(t)$ and $H_2(t)$:

$$\begin{aligned} H_1(t) &= H_V \cos(\omega t), \\ H_2(t) &= H_V \sin(\omega t), \end{aligned} \quad (2)$$

where $\omega = 2\pi f$ is the angular velocity of the rotating field vector \mathbf{H} . The maximum amplitude of both fields is equal to $H_V = 100 \text{ Oe}$, a value typical of hyperthermia applications [9,45].

The magnetic response of the system due to the effect of the rotating field is determined by solving magnetic rate equations applied to the magnetite nanoparticles pictured as two-level systems [double well systems (DWSs)]. The features, advantages, and limits of the rate-equation model have been discussed in detail elsewhere [29,57]; a concise summary of the method may be found in the Supplemental Material [58].

Although our final aim is to study the general case of nanoparticles characterized by a random distribution of easy axes in space, which closely fits the actual arrangement of easy axes of noninteracting nanoparticles dispersed in living tissue, it can be useful to start with a study of a planar distribution of easy axes. In this case, the easy axes are considered to lie in the x - y plane where the rotating field acts (i.e., $\alpha = \pi/2$); they are uniformly distributed around the z axis, with the ϕ angle taking all values between 0 and 2π . Studying the in-plane distribution of easy axes allows one to determine the released power density in a simple configuration; the results will be helpful in approaching the three-dimensional (3D) case.

A. In-plane distribution of easy axes

The magnetization of the nanoparticles is determined by thermally activated energy-barrier crossing in the presence of a cyclic magnetic field [46]. In order to obtain the magnetization in the rate-equation framework, the first step is to find the values and the angular positions of the two potential-energy minima for the magnetic moment and of the maximum between them (see Fig. 2, where the main features of the DWS model are sketched). These values are found by searching for the stationary points with respect to θ ($(\partial E/\partial\theta) = 0$) of the magnetic energy:

$$E(\theta, \phi, t) = K_{\text{eff}}V \sin^2(\phi - \theta) - M_S V H_1(t) \cos \theta - M_S V H_2(t) \sin \theta, \quad (3)$$

where $V = (\pi/3)D^3$ is the nanoparticle volume. For any angle ϕ_0 , the shape of the $E(\theta, \phi_0, t)$ curve cyclically evolves with time (the curve drawn as an example in the left-hand panel of Fig. 2 actually corresponds to $\phi_0 = \pi/6$ when $t = 0$). Once the values E_{m1} , E_{m2} , E_M , θ_1 , and θ_2 have been determined for each time, the quantities τ_1 and

τ_2 involved in the rate equations (see the Supplemental Material [58]) are easily obtained as

$$\begin{aligned} \tau_1(t) &= \tau_0 \exp\left(\frac{E_M - E_{m1}}{k_B T}\right), \\ \tau_2(t) &= \tau_0 \exp\left(\frac{E_M - E_{m2}}{k_B T}\right), \end{aligned} \quad (4)$$

where $\tau_0 \approx 1 \times 10^{-9} \text{s}$, k_B is the Boltzmann constant and $T = 300 \text{K}$. A significant quantity related to the τ_i values is the effective relaxation time τ_{eff} :

$$\tau_{\text{eff}} = \frac{\tau_1 \tau_2}{\tau_1 + \tau_2}, \quad (5)$$

which plays a role similar to the Néel relaxation time τ_N [32].

Let us now consider the subset of N_ϕ nanoparticles characterized by the same ϕ angle. The quantities τ_1^{-1} and τ_2^{-1} are the jump frequencies for energy-barrier crossing of the magnetic moment from well 1 to well 2 (and vice versa) and account for the combined effect of temperature and of the ac magnetic field [46]. The time-dependent occupancy parameters $n_{\phi 1} = N_{\phi 1}/N_\phi$ and $n_{\phi 2} = N_{\phi 2}/N_\phi$, which measure the degree of filling of each potential-energy well, are found by solving the rate equations [59]. Using the actual values of $n_{\phi 1}$ and $n_{\phi 2}$ and exploiting the standard procedure outlined elsewhere [57], it is possible to obtain the projections of the magnetization vector along the directions of the orthogonal fields $M_{\phi,1}(t)$ and $M_{\phi,2}(t)$. The magnitude $M_{\text{rot}}(\phi, t)$ and phase $\beta(\phi, t)$ of the rotating \mathbf{M}_ϕ vector are immediately found as follows:

$$\begin{aligned} M_{\text{rot}}(\phi, t) &= [M_{\phi,1}^2 + M_{\phi,2}^2]^{1/2}, \\ \beta(\phi, t) &= \arctan\left(\frac{M_{\phi,2}}{M_{\phi,1}}\right). \end{aligned} \quad (6)$$

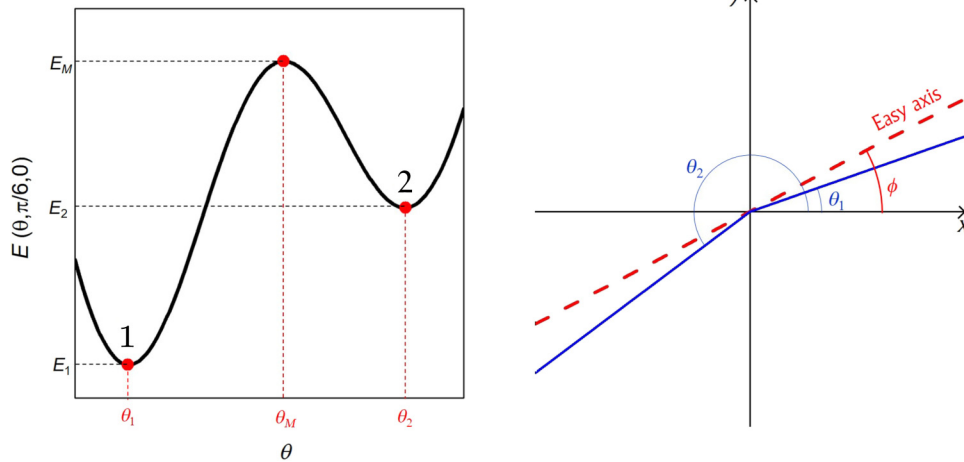


FIG. 2. Typical parameters of the DWS model for magnetite particles the easy axis of which lies in the x - y plane. In this example, the easy axis makes an angle $\phi_0 = \pi/6$ with the x axis.

The quantity $\beta(\phi, t)$ is the angle swept by the rotating magnetization of the considered subset of nanoparticles (in contrast, the angle swept by the rotating magnetic field is simply $\beta_H = \omega t$). The quantity:

$$\delta(\phi, t) = [\beta(\phi, t) - \beta_H(t)] = [\beta(\phi, t) - \omega t] \quad (7)$$

is the phase angle between the rotating magnetization of the considered subset and the field. Finally, the magnitude and the phase lag of the entire planar system of nanoparticles are obtained by integrating the ϕ -dependent quantities over the entire range of ϕ values:

$$\begin{aligned} M_{\text{rot}} &= \frac{1}{2\pi} \int_0^{2\pi} M_{\text{rot}}(\phi, t) d\phi \equiv \frac{1}{\pi} \int_0^{\pi} M_{\text{rot}}(\phi, t) d\phi, \\ \delta &= \frac{1}{2\pi} \int_0^{2\pi} \delta(\phi, t) d\phi \equiv \frac{1}{\pi} \int_0^{\pi} \delta(\phi, t) d\phi. \end{aligned} \quad (8)$$

The equivalence between the integrals in the two equations stems from the uniaxial (rather than unidirectional) symmetry of magnetic anisotropy. Performing the averages over ϕ cancels out the time dependence of both the integrand functions in Eq. (8). The results are displayed on a polar graph in Fig. 3(a), where the instantaneous arrangement of the \mathbf{H} and \mathbf{M}_{rot} vectors is shown for some values of the nanoparticle diameter when the time t is equal to an integer number of periods of the driving field. In this case, the vector \mathbf{H} is directed along 0° and the constant magnitude at all angles is rendered by the dotted circumference in black. The dashed circumferences in color refer to the magnitude of the \mathbf{M}_{rot} vector and indicate that M_{rot} , as obtained from Eq. (8), is the same for all angles swept by the vector; however, it can be noted that such a quantity is strongly dependent on the particle size. The \mathbf{M}_{rot} vector is in general delayed by a finite phase angle δ with respect to \mathbf{H} . Such a delay can be either almost insignificant, as for particles with $D = 11\text{--}12$ nm, or quite substantial, as for those with $D = 13\text{--}14$ nm.

It can be concluded that the \mathbf{M}_{rot} vector rotates in the x - y plane with the same angular velocity ω of the rotating field, with constant (size-dependent) magnitude and with a constant (size-dependent) lag with respect to \mathbf{H} .

The behavior of M_{rot} with D is shown in Fig. 3(b). For small D values, M_{rot} increases with the particle diameter because under the same H_V , the magnetic response is stronger in nanoparticles with a higher magnetic moment $M_s V$ (i.e., their magnetic susceptibility increases as D^3). However, such a trend is effectively contrasted and finally dominated by a strong reduction of the magnetic response of the system, because of the increase of the barrier between potential energy wells, which hinders the redistribution of the population between the two wells [46], finally leading to a very low asymptotic value of M_{rot} .

As expected, the phase lag δ is intrinsically related to the Néel relaxation of nanoparticles. The behavior of δ

with the effective relaxation time τ_{eff} [Eq. (5)] is reported in Fig. 3(c), where the diameters of nanoparticles associated with the τ_{eff} values are also shown. The maximum of δ is coincident with the period of the rotating field, $\mathcal{T} = 1/f$: this corresponds to the condition of maximum interference of the thermally activated redistribution of the populations between the two potential-energy minima with that induced by the rotating field [46]. When $\tau_{\text{eff}} \ll \mathcal{T}$, the thermally activated redistribution is so fast that the system is always at equilibrium and the resulting magnetization stays in phase with the field. On the other hand, when $\tau_{\text{eff}} \gg \mathcal{T}$, there is hardly any activated redistribution of the populations of the two wells and the magnetization is only related to the cyclic change of the tilt angles, θ_1 and θ_2 , by an effect of the rotation of \mathbf{H} . Such an effect, which does not involve any energy-barrier crossing, is almost instantaneous, so that again the phase lag disappears.

B. Power density released by a two-dimensional (2D) distribution of easy axes

The cyclic variation of the magnetic contribution to the internal energy ΔU_m over one full period of the magnetic field (i.e., one full rotation of the vector \mathbf{H} in the x - y plane) is (in Gaussian units [60])

$$\Delta U_m = \frac{1}{4\pi} \oint \mathbf{H} \cdot d\mathbf{B} \equiv \oint \mathbf{H} \cdot d\mathbf{M}, \quad (9)$$

the integral $\oint \mathbf{H} \cdot d\mathbf{H}$ being identically zero because $d\mathbf{H}$ is always $\perp \mathbf{H}$ in this case. On the basis of the results obtained in Sec. III A, the time behavior of \mathbf{H} and \mathbf{M} is

$$\begin{aligned} \mathbf{H}(t) &= H_V [\cos(\omega t) \mathbf{u}_x + \sin(\omega t) \mathbf{u}_y], \\ \mathbf{M}(t) \equiv \mathbf{M}_{\text{rot}}(t) &= M_{\text{rot}} [\cos(\omega t - \delta) \mathbf{u}_x + \sin(\omega t - \delta) \mathbf{u}_y] \end{aligned} \quad (10)$$

where \mathbf{u}_x and \mathbf{u}_y are unit vectors along the x and y axes, M_{rot} is a constant, and δ (a positive constant) is the time lag between \mathbf{M} and \mathbf{H} [Eqs. (7) and (8)]. Using

$$d\mathbf{M}(t) = \omega M_{\text{rot}} [-\sin(\omega t - \delta) \mathbf{u}_x + \cos(\omega t - \delta) \mathbf{u}_y] dt$$

and transforming the closed integral of Eq. (9) into an integral over one full period \mathcal{T} , one easily obtains

$$\begin{aligned} \Delta U_m &= H_V M_{\text{rot}} \omega \\ &\times \int_0^{\mathcal{T}} [-\sin(\omega t - \delta) \cos(\omega t) \cos(\omega t - \delta) \sin(\omega t)] dt \\ &= 2\pi H_V M_{\text{rot}} \sin \delta. \end{aligned}$$

Such an increase of the magnetic contribution to the total internal energy of the system of nanoparticles must be exactly counterbalanced by an energy transfer from the

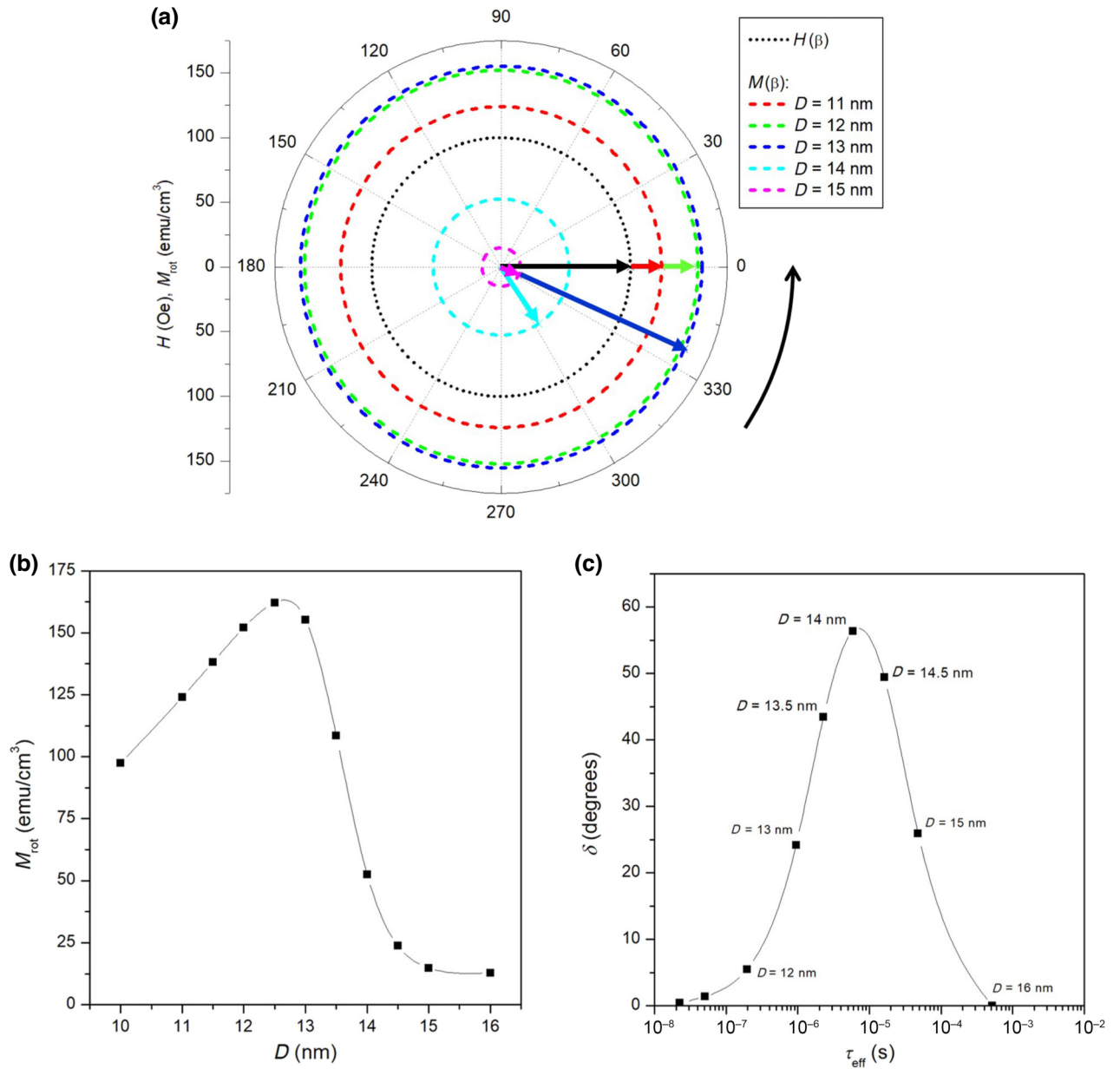


FIG. 3. (a) A polar graph of the rotating field and of the resulting magnetization for different nanoparticle sizes (see text). (b) The magnitude of the rotating magnetization vector \mathbf{M}_{rot} as a function of the nanoparticle diameter D . (c) The phase lag between the rotating magnetization and the field as a function of the effective relaxation time τ_{eff} of the DWS model. In-plane distribution of easy axes.

nanoparticles to the host tissue in the form of heat. The intrinsic heating power density of nanoparticles with easy axes distributed on the x - y plane is therefore

$$P_{2D} = 2\pi f H_V M_{\text{rot}} \sin \delta = \omega H_V M_{\text{rot}} \sin \delta, \quad (11)$$

where f is the common frequency of the harmonic orthogonal fields. Therefore, the released power is dependent on both M_{rot} and δ ; the overall behavior of the intrinsic power is shown in Fig. 4 as a function of the nanoparticle

diameter for the in-plane distribution of easy axes and for size-independent magnetic properties (full squares and full line). The curve turns out to be almost symmetrical around its maximum and is determined by the interplay between the behavior of M_{rot} and δ with D , as shown in Fig. 3.

C. Three-dimensional (3D) distribution of easy axes

In general, the easy axes of an assembly of nanoparticles embedded in living tissue or a phantom are randomly

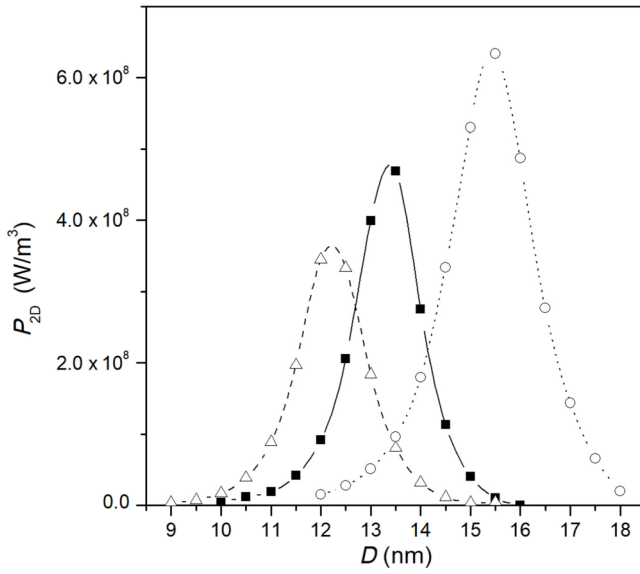


FIG. 4. The behavior with diameter D of the intrinsic power density P_{2D} generated by magnetite nanoparticles with easy axes in the x - y plane: full squares and full line, size-independent magnetic properties of particles; open circles and dotted line, size-dependent properties [case (a) of the Appendix]; open triangles and dashed line, size-dependent properties [case (b) of the Appendix].

directed along all directions in space, i.e., they are characterized by angles α and ϕ taking all values between 0 and π and between 0 and 2π , respectively. The magnetic response of nanoparticles is expected to be strongly influenced by α .

For example, the subset of nanoparticles with $\alpha = 0$ has the easy axis always perpendicular to the rotating field. In such a case, there is no redistribution of the population of the considered subset between the two wells (see Ref. [59]) and the magnetization vector is simply tilted from the z axis toward the instantaneous direction of the field in the x - y plane by the angle $\tilde{\theta} = \arcsin(M_S H_v / 2K_{\text{eff}})$. Therefore, the magnetization always lies in the plane determined by the z axis and the instantaneous direction of \mathbf{H} . In other words, the magnetization of these nanoparticles precedes with angular velocity ω around the z axis, describing a cone of aperture $2\tilde{\theta}$ with no phase lag with respect to the field; therefore, these nanoparticles do not contribute to the generation of heat.

Let us now consider the nanoparticles characterized by a fixed arbitrary value of α and all values of ϕ . For such a configuration, it is possible to introduce a plane $\Pi_{//}$ defined by the easy axis and the x axis and a plane Π_{\perp} that intersects $\Pi_{//}$ at right angles (see Fig. 5). The \mathbf{H} vector rotates in the x - y plane that forms the angle $(\pi/2 - \alpha)$ with $\Pi_{//}$; the projections on the $\Pi_{//}$ and Π_{\perp} planes of the circumference swept by the tip of the field vector are ellipses.

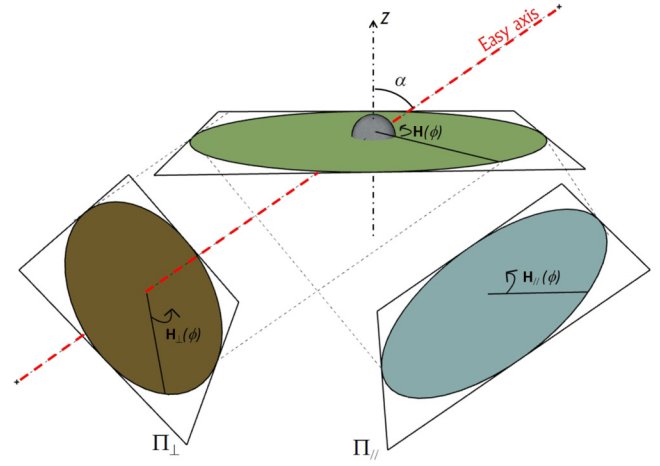


FIG. 5. The parallel ($H_{//}$) and perpendicular (H_{\perp}) field components acting on particles the easy axis of which makes a generic angle α with the z axis.

It should be recognized that the element of the magnetization produced by the \mathbf{H}_{\perp} component (see Fig. 5) does not lag the magnetic field (by the reasons outlined in Ref. [59]); only the component of the magnetization produced by $\mathbf{H}_{//}$ can have a phase lag with respect to the field due to the effect of the population redistribution between the two wells. As a consequence, when the aim is to determine the magnetic power dissipated by nanoparticles as heat—which only appears when the magnetization lags the field—the magnetization component related to the evolution of \mathbf{H}_{\perp} can be neglected. The magnetization arising from the evolution of $\mathbf{H}_{//}$ is instead first calculated for each ϕ , then averaged over all ϕ values, and finally projected on the x - y plane.

As a result, for each value of α , the only component of the magnetization that plays an active role in increasing the magnetic internal energy ΔU_m (and hence the generation of heat) is a vector $\mathbf{M}_{\text{rot}}(\alpha)$, which rotates in the x - y plane with angular velocity ω , as in the 2D case; the vector can be expressed in terms of the scalar quantities $M_{\text{rot}}(\alpha)$ and $\delta(\alpha)$ obtained as in Sec. III A [Eq. (8)]. These are reported in Fig. 6 for all α values between 0 and $\pi/2$ (it is sufficient to show such an interval because $M_{\text{rot}}(\pi/2 + \alpha) = M_{\text{rot}}(\pi/2 - \alpha)$ for symmetry reasons; the same condition applies to $\delta(\alpha)$).

For all nanoparticle diameters, the amplitude and phase lag of the rotating magnetization monotonically decrease when α decreases from $\pi/2$ to 0; for $D \geq 15$ nm, the variation of M_{rot} with α is small but nonzero, as shown by the horizontal black dashed line. It can be checked that for $\alpha = \pi/2$, the values of the 2D case are retrieved, while the phase lag $\delta(\alpha) \rightarrow 0$ for $\alpha \rightarrow 0$ for all diameters, as indeed expected.

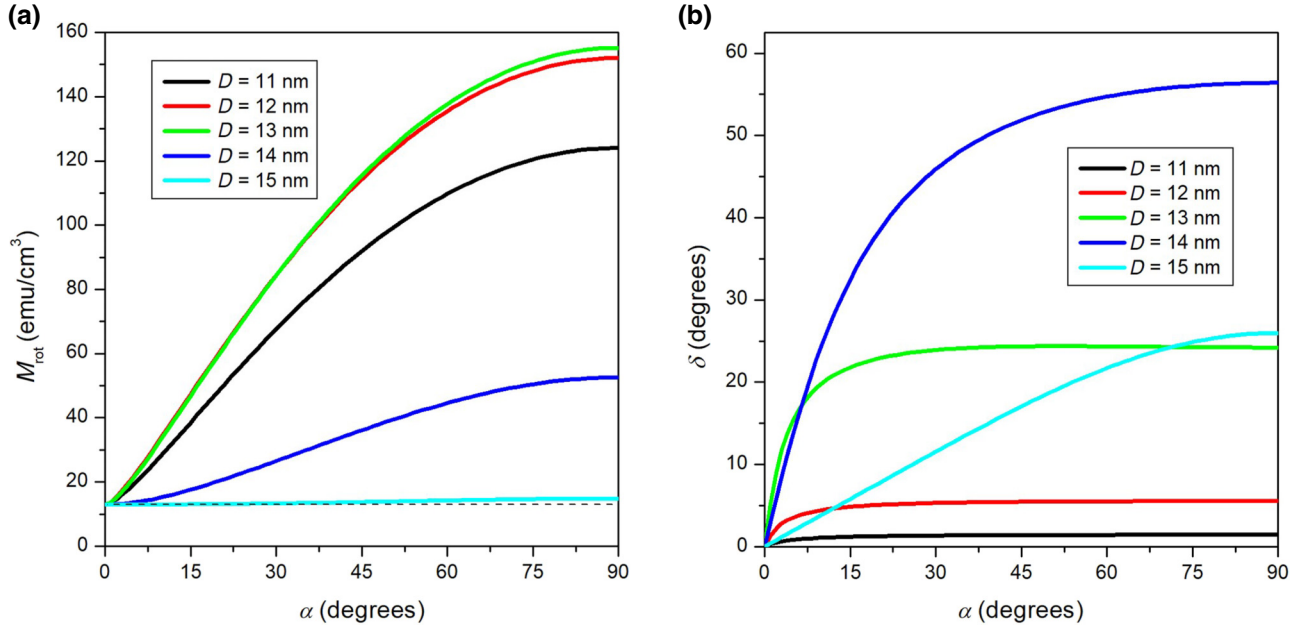


FIG. 6. (a) The behavior of the magnitude M_{rot} of the in-plane magnetization vector as a function of the angle α . (b) The same for the phase lag δ .

It should be stressed that the in-plane vector $\mathbf{M}_{\text{rot}}(\alpha)$ does not correspond to the whole magnetization of the system; however, all neglected magnetization components are either perpendicular to the \mathbf{H} vector or exactly in phase with it, therefore not contributing to the increase of ΔU_m . Therefore, the contribution of nanoparticles the easy axis of which makes the angle α with respect to the z axis has the same structure as discussed in Sec. III A except for the presence of an α -dependent magnitude and an α -dependent phase lag.

D. Power density released by a 3D distribution of easy axes

For each value of α , the intrinsic power density related to the lag between $\mathbf{M}_{\text{rot}}(\alpha)$ and \mathbf{H} is calculated following the same procedure as outlined in Sec. III B for the case $\alpha = \pi/2$. Therefore,

$$P_{2D}(\alpha) = 2\pi f H_V M_{\text{rot}}(\alpha) \sin \delta(\alpha). \quad (12)$$

The intrinsic power density arising from all the nanoparticles is obtained by integration:

$$\begin{aligned} P_{3D} &= \frac{1}{2} \int_0^\pi P_{2D}(\alpha) \sin(\alpha) d\alpha \\ &= \pi f H_V \int_0^\pi M_{\text{rot}}(\alpha) \sin(\delta(\alpha)) \sin(\alpha) d\alpha. \end{aligned} \quad (13)$$

It may be interesting to compare the intrinsic power density produced by nanoparticles of different size in a narrow

interval around any value of α ; to this aim, the quantity $P_{2D}(\alpha) \sin(\alpha)$ has been plotted in Fig. 7 in false colors on spherical polar graphs for D values ranging from 12 to 15 nm. These graphs are useful to single out the easy-axis directions corresponding to the maximum efficiency of nanoparticles as sources of heat; the results are obviously invariant under rotation around the z axis. The color scale in Fig. 7 is the same for all diameters and has been generated by normalizing the values taken by the quantity $P_{2D}(\alpha) \sin(\alpha)$ to its maximum value, observed to occur for $\alpha = \pi/2$ in nanoparticles with $D = 13$ nm. These polar graphs indicate that the heating performance of single-core magnetite nanoparticles is strongly dependent on their size and that their efficiency is highest when the easy axes are parallel to the plane where the magnetic field rotates.

The behavior of P_{3D} as a function of the nanoparticle diameter for $H_V = 100$ Oe, $f = 100$ kHz, and size-independent magnetic properties is shown in Fig. 8(a) (full black line and full symbols). The power density associated with the 3D distribution of easy axes keeps many of the features of the curve obtained for the in-plane distribution of easy axes (Fig. 4); this is not unexpected considering the procedure used to treat the 3D case. The function $P_{3D}(D)$ is again strongly peaked around the nanoparticle size for which $\tau_{\text{eff}} = 1/f$.

The advantage of replacing a linear harmonic field with a rotating field of the same amplitude and frequency is also shown in Fig. 8(a). The intrinsic power density of nanoparticles submitted to a driving field directed along an axis (red line and symbols) has been calculated by simply turning off the field $H_2(t)$. In this case, the behavior of $P_{3D}(D)$

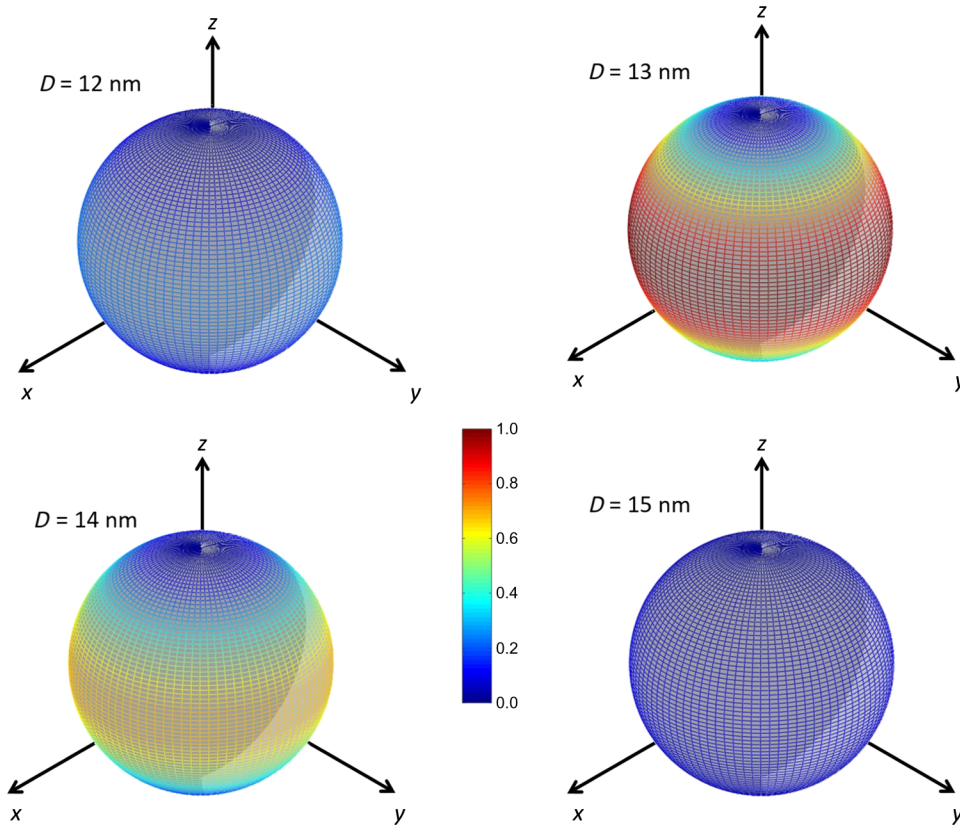


FIG. 7. Spherical polar graphs in false colors of the α -dependent intrinsic power density $P_{2D}(\alpha) \sin(\alpha)$, for some nanoparticle diameters. The color scale is the same in all graphs and represents values from 0 to 1 obtained by normalizing the plotted quantity to the maximum value (corresponding to $\alpha = \pi/2$ for $D = 13$ nm).

turns out to be similar to that arising from for the rotating field, except for the intensity of the maximum, which is definitely lower. The reason why magnetic nanoparticles are more efficient when they are excited by a rotating field is clarified in Fig. 8(b), where $P_{2D}(\alpha) \sin(\alpha)$ is plotted as a function of α in the two cases for the same nanoparticles ($D = 13$ nm). Under a rotating field, the largest contribution to the overall power density comes from particles the easy axis of which lies in, or makes a small angle with, the x - y plane ($\alpha \approx \pi/2$); on the contrary, such a contribution is almost suppressed when the driving field is applied along the x axis, which breaks the rotational symmetry around z typical of the rotating-field case.

E. Effect of vertex field and driving frequency

The results discussed in Sec. III D have been obtained for a vertex field of 100 Oe and a frequency of 100 kHz, representing the values usually dealt with in clinical applications of magnetic hyperthermia [45]. It may be useful to show the effect of changing these user-controlled quantities around the representative values. To this aim, one nanoparticle diameter has been selected

($D = 13.5$ nm, corresponding to the maximum of the P_{3D} curve in Fig. 8(a) (full squares and full line).

The effect of the vertex field on the intrinsic power density released by a 3D distribution of easy axes has been investigated in the interval $0 \leq H_V \leq 300$ Oe at $f = 100$ kHz. The results are reported in Fig. 9(a).

The function $P_{3D}(H_V)$ follows a H_V^2 law only for $H_V \lesssim 125$ Oe and displays a broad maximum around 200 Oe. Such behavior is explained in terms of competing contributions to the power density: with reference to Eqs. (12) and (13), it can be noted that the effect of increasing H_V (and consequently M_{rot}) is counterbalanced by a significant reduction of the lag $\delta(\alpha)$. The latter effect is explained by taking into account that a driving field of larger magnitude is more able to pull the magnetization away from the easy direction, resulting in a lesser time lag between $\mathbf{H}(t)$ and $\mathbf{M}_{rot}(t)$. Therefore, for a given frequency, the power released by the nanoparticles to the environment can be optimized by selecting the right amplitude of the rotating field. It should be noted that the H_V^2 dependence of the power density observed in Fig. 9 at small field amplitudes is also predicted by the linear-response theory for nanoparticles dispersed in a magnetic fluid [28,35,37,39]. The intrinsic power density released by the nanoparticles

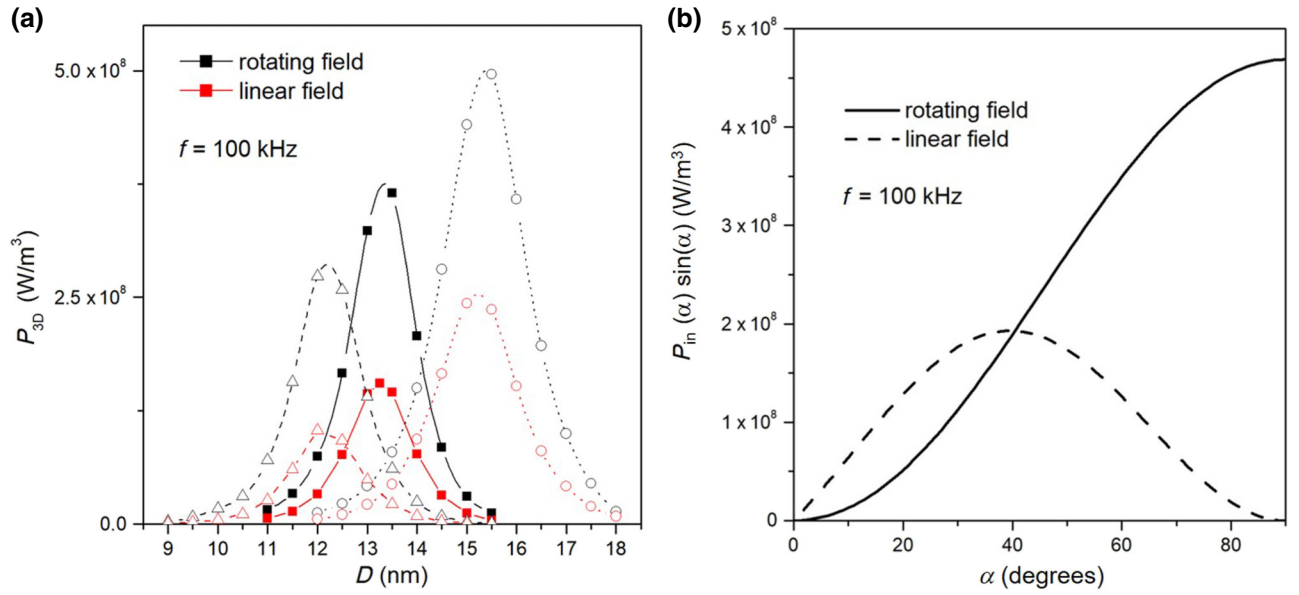


FIG. 8. (a) The intrinsic power density P_{3D} of magnetite nanoparticles of different size with easy axes randomly distributed in space and submitted to a rotating field with $H_V = 100$ Oe (black lines and symbols) and the same quantity obtained using a field of same frequency and amplitude directed along the x axis (red lines and symbols): full squares and full line, size-independent magnetic properties of particles; open circles and dotted lines, size-dependent properties [case (a) of the Appendix]; open triangles and dashed lines, size-dependent properties [case (b) of the Appendix]. (b) The behavior of the α -dependent power density for nanoparticles submitted to the rotating and to the linear field (full and dashed lines).

under a linear driving field of the same frequency is also shown. Using a rotating field is a more favorable option up to about 250 Oe; for higher field amplitudes, a crossover of the $P_{3D}(H_V)$ curves is observed, mainly owing to the fact

that the effects of the reduction of the lag between $\mathbf{H}(t)$ and $\mathbf{M}_{rot}(t)$ are not present when the excitation is provided by a linear field. However, for the driving-field amplitudes most commonly used in magnetic hyperthermia ($H_V < 250$ Oe

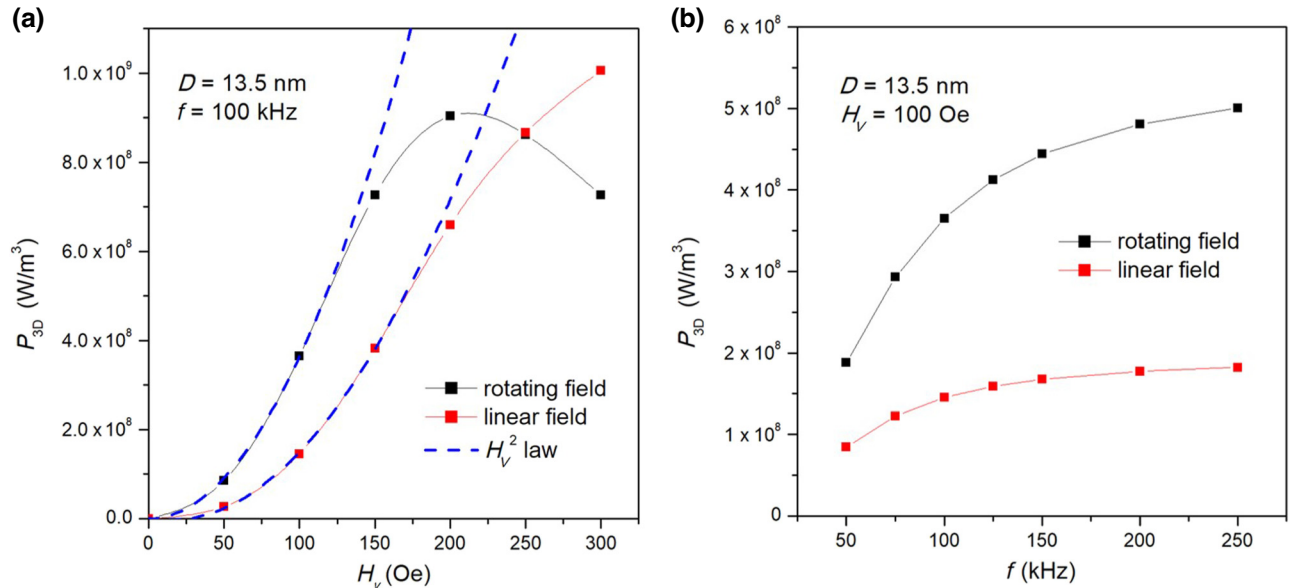


FIG. 9. (a) The intrinsic power density P_{3D} released by nanoparticles with $D = 13.5$ nm driven by a rotating and a linear driving field of frequency $f = 100$ kHz as a function of the vertex field H_V (black and red line and symbols); the dependence on the square of the field amplitude is shown for comparison (dashed blue lines). (b) The intrinsic power density P_{3D} released by the same nanoparticles as a function of frequency due to the effect of a rotating field (black line and symbols) and a linear field (red line and symbols) of the same amplitude ($H_V = 100$ Oe).

[14]), the rotating field ensures a better release of heating power by the nanoparticles. It should be recalled that in preclinical and clinical treatments at fixed frequency, the driving-field amplitude is to be kept as low as possible in order to meet the requirements of biological safety [14].

The effect of frequency on P_{3D} has been investigated in the interval $50 \text{ kHz} \leq f \leq 250 \text{ kHz}$ for $H_V = 100 \text{ Oe}$, as shown in Fig. 9(b). As expected, increasing the frequency results in larger values of P_{3D} ; however, the slope of the curve progressively decreases. This behavior is again explained in terms of competing effects on the power density; with reference to Eqs. (12) and (13), the enhancement of $P_{3D}(\alpha)$ arising from the contributions of both f and $\delta(\alpha)$ is attenuated by the decrease of M_{rot} , which is in turn related to the increasingly greater difficulty of the DWS to follow an increasingly fast rotating field. Such behavior differs from the f^2 dependence predicted by the linear-response theory applied to nanoparticles in magnetic fluids [39], where the magnetization processes do not involve an activated-barrier crossing. The intrinsic power density released by the nanoparticles under a linear driving field of the same amplitude is also shown; the rotating field is definitely the preferred solution in the whole interval of investigated frequencies, the advantage becoming increasingly pronounced with an increase in the frequency of the driving field.

IV. APPLICATION TO MAGNETIC HYPERTHERMIA

The input power density P_{in} in Eq. (1) is simply obtained by multiplying the intrinsic power density P_{3D} [Eq. (13)] by the volume fraction f_V of nanoparticles dispersed in the phantom:

$$P_{\text{in}} = P_{3D} f_V. \quad (14)$$

This input power density (the released power per unit volume of the tissue) is, of course, directly proportional to the SLP (the released power per unit mass of magnetic nanomaterial). When P_{in} is independent of the temperature, Eq. (1) is immediately solved in steady-state conditions. The final temperature increment above T_0 in the phantom of radius b is characterized by a parabolic profile:

$$T(r, \infty) = \frac{P_{\text{in}}}{6k} (b^2 - r^2) + \frac{P_{\text{in}} b}{3h},$$

where h is the convective heat transfer coefficient, which takes values of the order of $5 \times 10^4 \text{ Wm}^{-3} \text{ K}^{-1}$ in malignant tissues [9]. The maximum temperature increment is found in $r = 0$ and is $T_{\text{max}} = P_{\text{in}} b^2 / 6k + P_{\text{in}} b / 3h$; the temperature increment at the outer surface of the phantom is $T_b = P_{\text{in}} b / 3h$. The average steady-state temperature increment within the phantom turns out to be directly

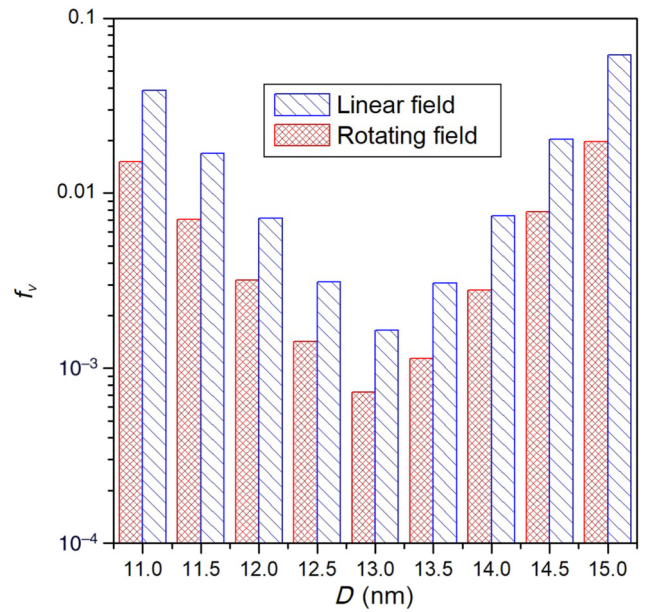


FIG. 10. The favorable effect of the rotating field on the dose of magnetite nanoparticles needed to increase the temperature of a target by 10°C , for different particle sizes.

proportional to the input power density:

$$T_{\text{ave}}(\infty) = \left[\frac{b}{9k} + \frac{1}{3h} \right] b P_{\text{in}} \approx 4.2 \times 10^{-5} P_{3D} f_V. \quad (15)$$

Here, the proportional constant is derived from the values of the parameters of the thermal model.

The volume concentration of nanoparticles needed to attain a given average temperature increment in the phantom (in this case, $T_{\text{ave}} = 10^\circ \text{C}$) is easily obtained from Eq. (15) and is shown in Fig. 10. Applying a uniformly rotating field reduces the local nanoparticle concentration needed to obtain the desired result, quite independently of the nanoparticle size. In fact, driving magnetic nanoparticles by a uniformly rotating magnetic field allows one to increase the heating efficiency with respect to a field applied along the x axis by a factor the average value of which in the considered set of nanoparticle diameters is about 2.5. As a consequence, the volume concentration of particles needed to achieve the same target temperature under the frequency and amplitude of the same field is reduced on average by the same factor; i.e., it is more than halved.

V. CONCLUSIONS

Enhancement of the heating efficiency of magnetite nanoparticles is an issue that is still a matter of concern in antitumor therapies based on magnetic particle hyperthermia. The SLP of magnetic particles can be increased by acting on the particles themselves (e.g., by using advanced

chemical methods to suitably modify their size, shape, or degree of aggregation) or by optimizing the field needed to drive their magnetization at high frequency, without the need to modify the properties and features of the magnetite nanoparticles obtained by standard preparation methods and/or available on the market and approved for medical use.

In magnetic particle hyperthermia, the magnetite nanoparticles are usually submitted to a harmonic field that is directed along a given axis; however, we have shown that such a configuration is not the best one in the case of nanoparticles distributed over a volume and that changing the geometry of the applied magnetic field from linear to circular—all other parameters being constant—permits us to more than double the heating efficiency of magnetic nanoparticles for hyperthermia. As a direct consequence, applying a uniformly rotating field reduces, by a factor larger than 2, the dose needed to attain a given target temperature in the malignant tissue. This result does not depend on the behavior with size of the intrinsic magnetic properties of nanoparticles. This can be a significant improvement because of the expected reduction of the adverse side effects related to nanoparticle biodistribution and clearance. From the standpoint of clinical safety, we should recall that a rotating field can be viewed as the superposition of two mutually orthogonal linear fields of the same frequency with a 90° phase shift. As a consequence, possibly harmful effects on healthy tissue are expected to roughly double in comparison to the linear-field case. For $f = 100$ kHz and $H_V = 100$ Oe, the detrimental effects of the rotating-field technique are still within the accepted safety limits.

Such a result has been obtained for nanoparticles characterized by the Néel relaxation mechanism. This is a realistic assumption when the nanoparticles, submitted to driving-field frequencies typical of actual hyperthermia therapy, have reached their positions in the target tissue where they are assumed to be physically constrained; however, this problem is difficult to treat owing to the intrinsic nonlinearity of the relation between the characteristic energies of the DWS and the relaxation times for the redistribution of magnetic moments in the two wells. The proposed magnetic model permits us to solve the problem in a satisfactory way and results in a remarkably simple revealing expression for the input power density P_{in} , which is directly proportional to the SLP.

APPENDIX: SIZE DEPENDENT MAGNETIC PROPERTIES

The surface properties of magnetic nanoparticles are often observed to reduce the magnetization and to enhance the effective anisotropy [48,53–55]. The effect—which is reduced or even disappears in almost ideal particles specially designed for proof-of-concept experiments

[49,50,52]—is usually accounted for by the following simple expressions [53,56]:

$$\begin{aligned} M_s(D) &= M_s^{(\text{bulk})} (1 - 2t/D)^3, \\ K_{\text{eff}}(D) &= K_V + \frac{6K_s}{D}, \end{aligned} \quad (\text{A1})$$

where $M_s^{(\text{bulk})}$ is the magnetization of bulk magnetite ($92 \text{ emu/g} = 478 \text{ emu/cm}^3$), t is the thickness of the magnetically dead layer at the nanoparticle surface [53,61], K_V is the bulk value of magnetic anisotropy, and K_s is the surface anisotropy [49,53,56].

In the following, it is assumed that t is of the order of 1 nm for all considered nanoparticle diameters, while the K_V and K_s parameters are taken from measurements on magnetite particles the size of which corresponds to the range of values considered here ($D \geq 9$ nm). In particular, the following two sets of values are used: (a) $K_V = 1.68 \times 10^5 \text{ erg/cm}^3$ and $K_s = 0.010 \text{ erg/cm}^2$ and (b) $K_V = 2.40 \times 10^5 \text{ erg/cm}^3$ and $K_s = 0.029 \text{ erg/cm}^2$. The first set is derived from the measurements by Nayek *et al.* [48], while the second one is given by Battle *et al.* [49] and applies to high-quality particles. It is worth noting that the constant value of K_{eff} used in this paper is halfway between the mean values in the interval of 9–16 nm calculated for case (a), $\bar{K}_{\text{eff}} = 2.19 \times 10^5 \text{ erg/cm}^3$, and for case (b), $\bar{K}_{\text{eff}} = 3.84 \times 10^5 \text{ erg/cm}^3$. The mean value of M_s is $\bar{M}_s = 332 \text{ emu/cm}^3$, close to the one used in this paper, $M_s = 350 \text{ emu/cm}^3$. This indicates that the constant values considered in this work are appropriate.

The values of P_{2D} obtained in both cases are reported in Fig. 4. The main properties of the curve obtained using constant magnetic parameters are retrieved; in particular, a sharp maximum of the intrinsic power density on the x - y plane is always observed. The maximum of the $P_{2D}(D)$ curve is displaced toward the right in case (a) (open circles and dotted line) and toward the left in case (b) (open triangles and dashed line) with respect to the value calculated using size-independent magnetic properties; a minor effect on the full width at half maximum of the curves is also observed. A remarkable result is the enhancement of the maximum of P_{2D} in case (a) and the corresponding reduction in case (b), with respect to the value obtained in Sec. III B. Both the shift of the curves and the behavior of the maximum are consistent with the fact that in cases (a) and (b), the mean values \bar{K}_{eff} are, respectively, higher and lower than $K_{\text{eff}} = 3 \times 10^5 \text{ erg/cm}^3$.

The effect of the size-dependent magnetic properties on the $P_{2D}(D)$ curve is mirrored in the behavior of the power density P_{3D} of nanoparticles with easy axes randomly distributed in space, as shown in Fig. 8 for both cases (a) and (b) (open circles and dotted line, and open triangles and dashed line, respectively). The variation of M_s and K_{eff} with size results in effects closely similar to the 2D case. Even when the intrinsic magnetic properties are size

dependent, the power density generated by nanoparticles under a rotating field overcomes, by more than a factor of 2, the same quantity produced by a field of the same frequency and amplitude directed along the x axis.

- [1] Q. A. Pankhurst, J. Connolly, S. K. Jones, and J. Dobson, Applications of magnetic nanoparticles in biomedicine, *J. Phys. D: Appl. Phys.* **36**, R167 (2003).
- [2] Q. Pankhurst, N. Thanh, S. Jones, and J. Dobson, Progress in applications of magnetic nanoparticles in biomedicine, *J. Phys. D: Appl. Phys.* **42**, 224001 (2009).
- [3] D. Rivera, A. J. Schupper, A. Bouras, M. Anastasiadou, L. Kleinberg, D. L. Kraitchman, A. Attaluri, R. Ivkov, and C. G. Hadjipanayis, Neurosurgical applications of magnetic hyperthermia therapy, *Neurosurg. Clin.* **34**, 269 (2023).
- [4] X. Liu, Y. Zhang, Y. Wang, W. Zhu, G. Li, X. Ma, Y. Zhang, S. Chen, S. Tiwari, K. Shi, *et al.*, Comprehensive understanding of magnetic hyperthermia for improving antitumor therapeutic efficacy, *Theranostics* **10**, 3793 (2020).
- [5] H. Gavilán, S. K. Avugadda, T. Fernández-Cabada, N. Soni, M. Cassani, B. T. Mai, R. Chantrell, and T. Pellegrino, Magnetic nanoparticles and clusters for magnetic hyperthermia: Optimizing their heat performance and developing combinatorial therapies to tackle cancer, *Chem. Soc. Rev.* **50**, 11614 (2021).
- [6] D. Dhar, S. Ghosh, S. Das, and J. Chatterjee, A review of recent advances in magnetic nanoparticle-based theranostics of glioblastoma, *Nanomedicine* **17**, 107 (2022).
- [7] A. Rajan and N. K. Sahu, Review on magnetic nanoparticle-mediated hyperthermia for cancer therapy, *J. Nanopart. Res.* **22**, 1 (2020).
- [8] S. Dutz and R. Hergt, Magnetic particle hyperthermia—a promising tumour therapy?, *Nanotechnology* **25**, 452001 (2014).
- [9] G. Barrera, P. Allia, and P. Tiberto, Temperature-dependent heating efficiency of magnetic nanoparticles for applications in precision nanomedicine, *Nanoscale* **12**, 6360 (2020).
- [10] S. V. Spirou, M. Basini, A. Lascialfari, C. Sangregorio, and C. Innocenti, Magnetic hyperthermia and radiation therapy: Radiobiological principles and current practice, *Nanomaterials* **8**, 401 (2018).
- [11] I. Raouf, S. Khalid, A. Khan, J. Lee, H. S. Kim, and M.-H. Kim, A review on numerical modeling for magnetic nanoparticle hyperthermia: Progress and challenges, *J. Therm. Biol.* **91**, 102644 (2020).
- [12] M. Suleman, S. Riaz, and R. Jalil, A mathematical modeling approach toward magnetic fluid hyperthermia of cancer and unfolding heating mechanism, *J. Therm. Anal. Calorim.* **146**, 1193 (2021).
- [13] G. Barrera, P. Allia, and P. Tiberto, Multifunctional effects in magnetic nanoparticles for precision medicine: Combining magnetic particle thermometry and hyperthermia, *Nanoscale Adv.* **5**, 4080 (2023).
- [14] L. Beola, L. Gutiérrez, V. Grauzú, and L. Asín, in *Nanomaterials for Magnetic and Optical Hyperthermia Applications* (Elsevier, Amsterdam, Netherlands, 2019), p. 317.
- [15] G. N. Rego, M. P. Nucci, J. B. Mamani, F. A. Oliveira, L. C. Marti, I. S. Filgueiras, J. M. Ferreira, C. C. Real, D. d. P. Faria, P. L. Espinha, *et al.*, Therapeutic efficiency of multiple applications of magnetic hyperthermia technique in glioblastoma using aminosilane coated iron oxide nanoparticles: In vitro and in vivo study, *Int. J. Mol. Sci.* **21**, 958 (2020).
- [16] M. M. Paulides, D. B. Rodrigues, G. G. Bellizzi, K. Sumser, S. Curto, E. Neufeld, H. Montanaro, H. P. Kok, and H. Dobsicek Trefna, ESHO benchmarks for computational modeling and optimization in hyperthermia therapy, *Int. J. Hyperth.* **38**, 1425 (2021).
- [17] H. Gavilán, K. Simeonidis, E. Myrovali, E. Mazarío, O. Chubykalo-Fesenko, R. Chantrell, L. Balcells, M. Angelakeris, M. Morales, and D. Serantes, How size, shape and assembly of magnetic nanoparticles give rise to different hyperthermia scenarios, *Nanoscale* **13**, 15631 (2021).
- [18] L. Nguyen, V. Oanh, P. Nam, D. Doan, N. Truong, N. Ca, P. Phong, L. Hong, and T. Lam, Increase of magnetic hyperthermia efficiency due to optimal size of particles: Theoretical and experimental results, *J. Nanopart. Res.* **22**, 1 (2020).
- [19] H. Etemadi and P. G. Plieger, Magnetic fluid hyperthermia based on magnetic nanoparticles: Physical characteristics, historical perspective, clinical trials, technological challenges, and recent advances, *Adv. Ther.* **3**, 2000061 (2020).
- [20] X. Yu, S. Ding, R. Yang, C. Wu, and W. Zhang, Research progress on magnetic nanoparticles for magnetic induction hyperthermia of malignant tumor, *Ceram. Int.* **47**, 5909 (2021).
- [21] K. Parekh, A. Bhardwaj, and N. Jain, Preliminary in vitro investigation of magnetic fluid hyperthermia in cervical cancer cells, *J. Magn. Magn. Mater.* **497**, 166057 (2020).
- [22] J. Nowak-Jary and B. Machnicka, In vivo biodistribution and clearance of magnetic iron oxide nanoparticles for medical applications, *Int. J. Nanomedicine* **479**, 4067 (2023).
- [23] J. Bourquin, A. Milosevic, D. Hauser, R. Lehner, F. Blank, A. Petri-Fink, and B. Rothen-Rutishauser, Biodistribution, clearance, and long-term fate of clinically relevant nanomaterials, *Adv. Mater.* **30**, 1704307 (2018).
- [24] L. Yang, H. Kuang, W. Zhang, Z. P. Aguilar, Y. Xiong, W. Lai, H. Xu, and H. Wei, Size dependent biodistribution and toxicokinetics of iron oxide magnetic nanoparticles in mice, *Nanoscale* **7**, 625 (2015).
- [25] A. Włodarczyk, S. Gorgoń, A. Radoń, and K. Bajdak-Rusinek, Magnetite nanoparticles in magnetic hyperthermia and cancer therapies: Challenges and perspectives, *Nanomaterials* **12**, 1807 (2022).
- [26] B. Herrero de la Parte, I. Rodrigo, J. Gutiérrez-Basoa, S. Iturrizaga Correcher, C. Mar Medina, J. J. Echevarría-Uraga, J. A. Garcia, F. Plazaola, and I. García-Alonso, Proposal of new safety limits for in vivo experiments of magnetic hyperthermia antitumor therapy, *Cancers* **14**, 3084 (2022).
- [27] R. Hergt and S. Dutz, Magnetic particle hyperthermia—biophysical limitations of a visionary tumour therapy, *J. Magn. Magn. Mater.* **311**, 187 (2007).

- [28] C. M. Lucaciu, S. Nitica, I. Fizesan, L. Filip, L. Bilteanu, and C. Iacovita, Enhanced magnetic hyperthermia performance of zinc ferrite nanoparticles under a parallel and a transverse bias dc magnetic field, *Nanomaterials* **12**, 3578 (2022).
- [29] P. Allia, G. Barrera, and P. Tiberto, Nonharmonic driving fields for enhancement of nanoparticle heating efficiency in magnetic hyperthermia, *Phys. Rev. Appl.* **12**, 034041 (2019).
- [30] M. Zeinoun, J. Domingo-Diez, M. Rodriguez-Garcia, O. Garcia, M. Vasic, M. Ramos, and J. J. Serrano Olmedo, Enhancing magnetic hyperthermia nanoparticle heating efficiency with non-sinusoidal alternating magnetic field waveforms, *Nanomaterials* **11**, 3240 (2021).
- [31] L. Souiade, J. Domingo-Diez, C. Alcaide, B. Gámez, L. Gámez, M. Ramos, and J. J. Serrano Olmedo, Improving the efficacy of magnetic nanoparticle-mediated hyperthermia using trapezoidal pulsed electromagnetic fields as an in vitro anticancer treatment in melanoma and glioblastoma multiforme cell lines, *Int. J. Mol. Sci.* **24**, 15933 (2023).
- [32] R. Hergt, R. Hiergeist, I. Hilger, W. A. Kaiser, Y. Lapatnikov, S. Margel, and U. Richter, Maghemite nanoparticles with very high ac-losses for application in rf-magnetic hyperthermia, *J. Magn. Magn. Mater.* **270**, 345 (2004).
- [33] H. Fatima, T. Charinpanitkul, and K.-S. Kim, Fundamentals to apply magnetic nanoparticles for hyperthermia therapy, *Nanomaterials* **11**, 1203 (2021).
- [34] P. Cantillon-Murphy, L. L. Wald, E. Adalsteinsson, and M. Zahn, Heating in the MRI environment due to superparamagnetic fluid suspensions in a rotating magnetic field, *J. Magn. Magn. Mater.* **322**, 727 (2010).
- [35] M. Beković, M. Trbušić, S. Gyergyek, M. Trlep, M. Jesenik, P. S. Szabo, and A. Hamler, Numerical model for determining the magnetic loss of magnetic fluids, *Materials* **12**, 591 (2019).
- [36] R. G. Gontijo and A. B. Guimarães, Langevin dynamic simulations of magnetic hyperthermia in rotating fields, *J. Magn. Magn. Mater.* **565**, 170171 (2023).
- [37] M. Beković, M. Trbušić, M. Trlep, M. Jesenik, and A. Hamler, Magnetic fluids' heating power exposed to a high-frequency rotating magnetic field, *Adv. Mater. Sci. Eng.* **2018**, 1 (2018).
- [38] M. Beković, M. Trlep, M. Jesenik, and A. Hamler, A comparison of the heating effect of magnetic fluid between the alternating and rotating magnetic field, *J. Magn. Magn. Mater.* **355**, 12 (2014).
- [39] A. Skumiel, P. Kopcansky, M. Timko, M. Molcan, K. Paulovicova, and R. Wojciechowski, The influence of a rotating magnetic field on the thermal effect in magnetic fluid, *Int. J. Therm. Sci.* **171**, 107258 (2022).
- [40] V. Sharapova, M. Uimin, A. Mysik, and A. Ermakov, Heat release in magnetic nanoparticles in ac magnetic fields, *Phys. Met. Metallogr.* **110**, 5 (2010).
- [41] A. Miaskowski and M. Subramanian, Numerical model for magnetic fluid hyperthermia in a realistic breast phantom: Calorimetric calibration and treatment planning, *Int. J. Mol. Sci.* **20**, 4644 (2019).
- [42] M. Ragab, A. E. Abouelregal, H. F. AlShaibi, and R. A. Mansouri, Heat transfer in biological spherical tissues during hyperthermia of magnetoma, *Biology* **10**, 1259 (2021).
- [43] H.-W. Huang and T.-L. Horng, in *Heat Transfer and Fluid Flow in Biological Processes* (Elsevier, London, UK, 2015), p. 1.
- [44] D. Soukup, S. Moise, E. Céspedes, J. Dobson, and N. D. Telling, *In situ* measurement of magnetization relaxation of internalized nanoparticles in live cells, *ACS Nano* **9**, 231 (2015).
- [45] G. P. Skandalakis, D. R. Rivera, C. D. Rizea, A. Bouras, J. G. Jesu Raj, D. Bozec, and C. G. Hadjipanayis, Hyperthermia treatment advances for brain tumors, *Int. J. Hyperthermia* **37**, 3 (2020).
- [46] G. Barrera, P. Allia, and P. Tiberto, Dipolar interactions among magnetite nanoparticles for magnetic hyperthermia: A rate-equation approach, *Nanoscale* **13**, 4103 (2021).
- [47] G. Barrera, P. Allia, and P. Tiberto, Magnetic tracers for magnetic particle imaging: Insight on the roles of frequency-sustained hysteresis and interactions in quantitative imaging, *Phys. Rev. Appl.* **19**, 034029 (2023).
- [48] C. Nayek, K. Manna, A. Imam, A. Alqasrawi, and I. Obaidat, in *IOP Conference Series: Materials Science and Engineering*, Vol. 305 (IOP Publishing, Bristol, UK, 2018), p. 012012.
- [49] X. Battle, N. Pérez, P. Guardia, O. Iglesias, A. Labarta, F. Bartolomé, L. García, J. Bartolomé, A. Roca, M. Morales, *et al.*, Magnetic nanoparticles with bulklike properties, *J. Appl. Phys.* **109**, 07B524 (2011).
- [50] H. Mamiya, H. Fukumoto, J. L. Cuya Huaman, K. Suzuki, H. Miyamura, and J. Balachandran, Estimation of magnetic anisotropy of individual magnetite nanoparticles for magnetic hyperthermia, *ACS Nano* **14**, 8421 (2020).
- [51] S. Oyarzún, A. Tamion, F. Tournus, V. Dupuis, and M. Hillenkamp, Size effects in the magnetic anisotropy of embedded cobalt nanoparticles: From shape to surface, *Sci. Rep.* **5**, 14749 (2015).
- [52] M. Unni, A. M. Uhl, S. Savliwala, B. H. Savitzky, R. Dhavalikar, N. Garraud, D. P. Arnold, L. F. Kourkoutis, J. S. Andrew, and C. Rinaldi, Thermal decomposition synthesis of iron oxide nanoparticles with diminished magnetic dead layer by controlled addition of oxygen, *ACS Nano* **11**, 2284 (2017).
- [53] P. Dutta, S. Pal, M. Seehra, N. Shah, and G. Huffman, Size dependence of magnetic parameters and surface disorder in magnetite nanoparticles, *J. Appl. Phys.* **105**, 07B501 (2009).
- [54] Z. Shaterabadi, G. Nabyouni, G. F. Goya, and M. Soleymani, The effect of the magnetically dead layer on the magnetization and the magnetic anisotropy of the dextran-coated magnetite nanoparticles, *Appl. Phys. A* **128**, 631 (2022).
- [55] K. Pisane, S. Singh, and M. Seehra, Unusual enhancement of effective magnetic anisotropy with decreasing particle size in maghemite nanoparticles, *Appl. Phys. Lett.* **110**, 222409 (2017).
- [56] F. Bødker, S. Mørup, and S. Linderorth, Surface effects in metallic iron nanoparticles, *Phys. Rev. Lett.* **72**, 282 (1994).

- [57] P. Allia, G. Barrera, and P. Tiberto, Hysteresis effects in magnetic nanoparticles: A simplified rate-equation approach, *J. Magn. Magn. Mater.* **496**, 165927 (2020).
- [58] See the Supplemental Material at <http://link.aps.org/supplemental/10.1103/PhysRevApplied.21.064037> for a summary of the DWS model and the rate-equation framework, and a brief discussion on the validity of the rate-equation approach.
- [59] A consequence of the DWS model is that only a magnetic field parallel to the easy axis able to cause a redistribution of the population of nanoparticles between the two wells but a perpendicular field does not affect the population, i.e., $n_{\phi_1} = n_{\phi_2} = 1/2$, and the magnetization turns out to be always in phase with the driving field (see Ref. [57]).
- [60] Gaussian units for the magnetic properties will be used throughout this paper; however, the resulting power density will be converted into SI units (W/m^3).
- [61] S. Pal, P. Dutta, N. Shah, G. Huffman, and M. Seehra, Surface spin disorder in Fe_3O_4 nanoparticles probed by electron magnetic resonance spectroscopy and magnetometry, *IEEE Trans. Magn.* **43**, 3091 (2007).